ACS APPLIED MATERIALS & INTERFACES

Research Article

www.acsami.org

All-Organic Sulfonium Salts Acting as Efficient Solution Processed Electron Injection Layer for PLEDs

Dimitra G. Georgiadou,*[,†,‡] Maria Vasilopoulou,[†] Leonidas C. Palilis,[§] Ioannis D. Petsalakis,[∥] Giannoula Theodorakopoulos,[∥] Vassilios Constantoudis,[†] Stella Kennou,[⊥] Antonis Karantonis,[‡] Dimitra Dimotikali,[‡] and Panagiotis Argitis*[,†]

[†]Institute of Microelectronics, NCSR "Demokritos", 15310 Athens, Greece

[‡]School of Chemical Engineering, National Technical University of Athens, 15780 Athens, Greece

[§]Department of Physics, University of Patras, 26500 Patras, Greece

[∥]Theoretical and Physical Chemistry Institute, The National Hellenic Research Foundation, 11635 Athens, Greece

[⊥]Department of Chemical Engineering, University of Patras, 26500 Patras, Greece

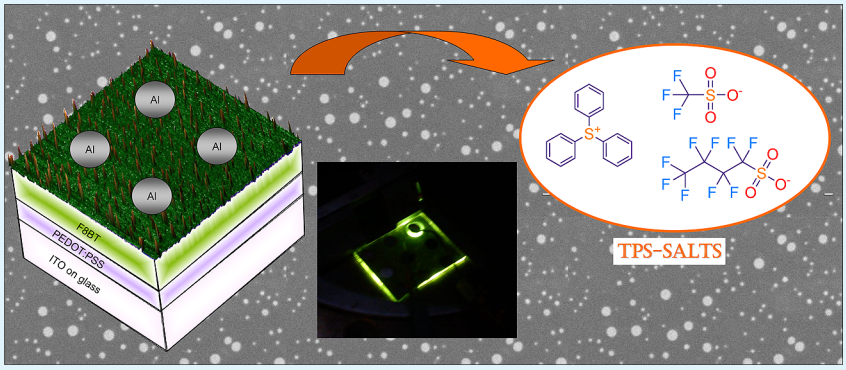

ABSTRACT: Herein we introduce the all-organic triphenylsulfonium (TPS) salts cathode interfacial layers (CILs), deposited from their methanolic solution, as a new simple strategy for circumventing the use of unstable low work function metals and obtaining charge balance and high electroluminescence efficiency in polymer light-emitting diodes (PLEDs). In particular, we show that the incorporation of TPS-triflate or TPS-nonaflate at the polymer/Al interface improved substantially the luminous efficiency of the device (from 2.4 to 7.9 cd/A) and reduced the turn-on and operating voltage, whereas an up to 4-fold increase in brightness (~11 250 cd/m^2 for TPS-triflate and ~14 682 cd/m^2 for TPS-nonaflate compared to ~3221 cd/m^2 for the reference device) was observed in poly[(9,9-dioctylfluorenyl-2,7-diyl)-*co*-(1,4-benzo-2,1′,3-thiadiazole)] (F8BT)-based PLEDs. This was mainly attributed to the favorable decrease of the electron injection barrier, as derived from the open-circuit voltage (V_{oc}) measurements, which was also assisted by the conduction of electrons through the triphenylsulfonium salt sites. Density functional theory calculations indicated that the total energy of the anionic (reduced) form of the salt, that is, upon placing an electron to its lowest unoccupied molecular orbital, is lower than its neutral state, rendering the TPS-salts stable upon electron transfer in the solid state. Finally, the morphology optimization of the TPS-salt interlayer through controlling the processing parameters was found to be critical for achieving efficient electron injection and transport at the respective interfaces.

KEYWORDS: *OLEDs, triflate, nonaflate, counterions, cathode interfacial layer, electron transport*

1. INTRODUCTION

The interest in polymer light emitting diodes (PLEDs) has increased in the last years, since the possibilities for facile fabrication renders them attractive candidates for large area lighting applications as well as solution-processed small size disposable displays.[1] For efficient low-power consuming devices, low work function metals are needed as cathodes (e.g., Ca, Ba, Mg). However, these are unstable in ambient environment due to oxidation of the metal and result in fast deterioration of the device performance, which is manifested via dark spot formation during operation and low lifetimes. On the other hand, the environmentally stable metals (e.g., Al, Ag) form large injection barriers with the polymer's lowest unoccupied molecular orbital (LUMO) level, which hampers the injection of electrons. Therefore, the need for devices with low operating voltage remains an open issue, and this has triggered the research on efficient electron injecting/transporting layers (EILs/ETLs).[2]

The most prominent material approaches presented so far as efficient EILs include insulating inorganic salts, such as alkaline

Received: July 23, 2013
Accepted: November 7, 2013
Published: November 7, 2013

fluorides (LiF,[3] CsF[4]), quinolines (Liq,[5] Csq[6]), NaOH,[7] and cesium salts (CsCl,[8] Cs_2CO_3[9]), inorganic metal oxides, either fully oxidized (e.g., ZrO_2,[10,11] ZnO[12]) or substoichiometric (WO_x, MoO_x),[13,14] while some organic molecules (e.g., siloles,[15] pyridines,[16,17] phenanthrolines,[18] etc.) with low lying LUMOs and high electron mobilities have also been used in high efficiency OLED devices. Nevertheless, in most of these cases, the material of the EIL is vacuum evaporated, which increases the complexity and the manufacturing cost. To address this issue, solution-processed inorganic salts, for example, Cs_2CO_3,[19] $Ba(OH)_2$, and barium acetylacetonate ($Ba(acac)_2$),[20] have been suggested as efficient hole blocking layers (HBLs) with electron transporting channels. Our group has also demonstrated the use of spin-coated inorganic semiconducting molecular oxides, that is, polyoxometalates (POMs),[21,22] and organic or metal−organic H_2- or Zn-porphyrins[23] as cathode interfacial layers (CILs) in organic optoelectronic devices achieving improved device performance.

On the other hand, ion conducting polymers such as poly(ethyleneoxide) (PEO),[24] PEGDE[25] or PEGDE/rubrene,[26] or even blends of an alkaline salt (e.g., Cs_2CO_3[27] or KCF_3SO_3[28]) or an anionic surfactant (e.g., sodium dodecyl sulfate)[29] with PEO have been suggested as solution processable interfacial layers. An alternative pathway involves the use of all-organic solution-deposited materials, such as properly functionalized conjugated polymers,[30,31] while Zhou et al. have proposed implementing amine-bearing large band gap polymeric surface modifiers that lower substantially the work function of several materials used as cathode electrodes in different optoelectronic devices.[32] In this direction, the most popular approach so far is based on the use of conjugated polymers with pendant ionic groups, the so-called conjugated polyelectrolytes (CPEs).[33] These may be anionic (e.g., polysulfonates with alkali or alkylammonium cations as counterions), cationic[34] (mainly alkylammonium or N-heterocyclic cations, like, e.g., imidazolium with corresponding halide anions), or even zwitterionic[35] (e.g., ammonium sulfonates without free counterions) or diblock[36] or triblock[37] copolymers. Recently, the importance of the conjugated nature of the polyelectrolytes used as electron injecting layers was put into question.[38−40] In fact, Min et al. reported on a small molecule zwitterionic compound without any π-delocalized unit, which showed excellent device performance.[39]

Organic salts, and more specifically "onium salts", such as ammonium-based cationic polyelectrolytes, are often employed as effective electron injecting layers for OLEDs,[41] whereas the small molecule "semiorganic" tetrabutylammonium hydroxide (TBA−OH) has been also proposed to act as efficient solution-processed electron injection layer in polufluorene-based PLED pixels fabricated with laser-induced forward transfer (LIFT).[42,43] Herein we introduce triphenylsulfonium (TPS) salts, deposited from a methanolic solution on top of a hydrophobic emissive layer, as a new class of all-organic ionic interface modifiers, which offer the advantage of low-cost process and easier synthesis compared to CPEs, to obtain charge balance and high electroluminescence efficiency in PLEDs. Sulfonium salts are a class of molecular compounds that have been widely used as photoinitiators in cationic polymerizations[44] and photoacid generators (PAGs) in lithographic imaging processes, where they were employed in catalyzing deprotection or cross-linking reactions in chemically amplified photoresists (see, e.g., refs 45 and 46). In a previous work of our group, we demonstrated that certain sulfonium salts, acting as photoacid generators, can be used in single layer PLEDs in order to achieve photochemically induced tuning of the emission color by protonation of emitter basic sites.[47,48] Motivated by this work, we decided to investigate the effect of adding triphenylsulfonium salts in the emissive layer, either the green-emitting poly[(9,9-dioctylfluorenyl-2,7-diyl)-*co*-(1,4-benzo-2,1′,3-thiadiazole)] (F8BT)[49] or the blue-emitting poly[2-(6-cyano-6-methyl-heptyloxy)-1,4-phenylene] (CN-PPP),[50,51] on the charge transport and emission properties of the device. A substantially ameliorated device performance was observed in both cases, mainly attributed to enhanced charge injection due to the ionic effect induced by the TPS-salts addition in the polymer matrix. However, in the particular case when a TPS salt was blended with the blue-emitting (wide band gap) polymer, their ability to aid the transport of electrons through the TPS LUMO was also unveiled. The latter observation prompted us to investigate the utilization of these compounds for the first time as solution-processed cathode interfacial layers in PLEDs.

In this Article, we present results with two triphenylsulfonium salts (differing in the anion size) deposited on top of F8BT from an orthogonal (with regard to the F8BT underlayer) solvent, and we show that these CILs facilitate electron injection and transport from an Al cathode to the F8BT emissive layer, leading to devices that outperform in terms of brightness and efficiency both the reference device and devices with TPS-salts blended with the light-emitting polymer. The optoelectronic characteristics of the diodes are correlated with the energetics of the TPS-salts and the formation of a favorably oriented dipole at the interface due to their polar nature, leading to a reduction of the energetic barrier for electron injection. Theoretical studies employing density functional theory (DFT) and time-dependent DFT (TD-DFT) calculations on the TPS-salts and their reduced form show that the injection of an electron is further stabilizing the TPS-salt molecule. Furthermore, the film forming properties of these materials are thoroughly investigated and it turns out that the morphology determines to a large extent the optimal performance of the PLED. The presented results highlight the suitability of these compounds to be incorporated as electron injecting layers in efficient, inexpensive, solution-processed organic electronic devices.

2. EXPERIMENTAL DETAILS

2.1. Materials. ITO-coated glass substrates (25 × 25 mm^2) with a sheet resistance of 20 Ω/square were obtained from Präzisions Glas & Optik. Poly(3,4-ethylenedioxythiophene):poly(styrenesulfonate) (PEDOT:PSS) (CLEVIOS P VP CH 8000) was provided by Heraeus Precious Metals. Poly[(9,9-dioctylfluorenyl-2,7-diyl)-*co*-(1,4-benzo-2,1′,3-thiadiazole)] (F8BT) green-emitting copolymer was purchased from American Dye Source. The sulfonium salts used were triphenylsulfonium trifluoromethanesulfonate (TPS-triflate) and triphenylsulfonium perfluoro-1-butanesulfonate (TPS-nonaflate) (see Figure 1), all obtained from Midori Kagaku. The supporting electrolyte tetrabutylammonium tetrafluoroborate (Bu_4NBF_4) was purchased from Sigma-Aldrich. All materials were used as received.

2.2. PLEDs Fabrication. ITO substrates were cleaned with detergent, deionized water, acetone, and isopropanol and then treated with O_2 plasma. A thin layer (40 nm) of PEDOT:PSS was formed upon spin-coating a prefiltered (through a 0.45 μm PVDF filter) aqueous solution on top of them to enhance hole injection and smoothen the ITO surface. PEDOT:PSS films were annealed at 135 °C for at least 15 min in air. The F8BT emitting layer was then spin-coated from an 8 mg/mL chloroform solution (prefiltered through a 0.20 μm PTFE filter), resulting in a film thickness of about 90 nm, and

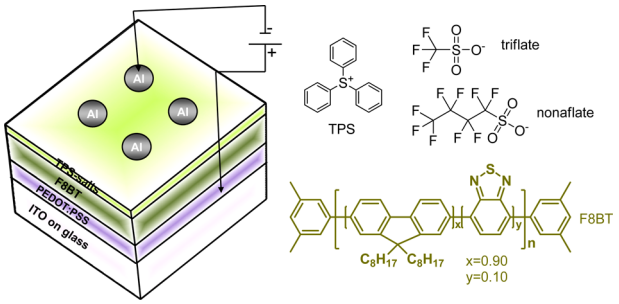

Figure 1. PLED device structure and chemical structure of the TPS-salts used and of the F8BT copolymer.

annealed at 80 °C for 10 min in air. The sulfonium salts were spin-coated at 2000 rpm onto the F8BT layer from different concentration solutions in methanol, an orthogonal solvent for typical semiconducting polymers, so that the hydrophobic emitting layer would not be influenced by the TPS-salt deposition. The devices were completed with a 150 nm thick aluminum cathode, deposited by thermal evaporation through a shadow mask (defined active area of 12.56 mm^2) in a dedicated chamber. Following Al deposition, the PLED samples were annealed at 110 °C for 15 min in air before measurement. All organic layer depositions were carried out in ambient conditions, and all device measurements were conducted immediately after their fabrication in air without any encapsulation.

2.3. Characterization. The valence band spectra of triphenylsulfonium salts were evaluated after recording the UV photoemission spectra (UPS) of films deposited on a 100 nm aluminum thick film, evaporated on a Si substrate. The UPS measurements were performed by using a Leybold EA11 hemispherical analyzer and the He I (21.2 eV) excitation line. A negative bias of 12.28 V was applied to the sample during UPS measurements to separate sample and analyzer high binding energy cutoff. Thin-film absorption spectra (on a quartz substrate) were recorded with a Perkin-Elmer Lamda 40 UV/vis spectrophotometer.

Cyclic voltammetry measurements were performed in 10^{-3} M solutions of the TPS salts in acetonitrile with the addition of 10^{-1} M Bu_4NBF_4. The working electrode was 1 mm diameter Pt wire, a Pt foil served as the counter electrode, and standard calomel electrode (SCE) in saturated KCl was the reference electrode. Measurements were recorded with a 263A EG&G PAR potensiostat and a DL708E YOKOGAWA oscilloscope. The LUMO energies of the TPS-salts were calculated from their (irreversible) reduction potential (vs SCE) by applying the relation:[52]

$$E_{\mathrm{LUMO}} = -(E^{\mathrm{red}}_{\mathrm{vsSCE}} + 4.8)\ \mathrm{eV}$$

Surface morphology was probed with an NT-MDT atomic force microscope (AFM) operated in tapping mode and a JEOL JSM 7401F scanning electron microscope (FE-SEM).

Current density−voltage (J−V) characteristics were measured with a Keithley 2400 source-measure unit, and luminance and EL spectral characteristics were recorded with an Ocean Optics spectrophotometer equipped with fiber optics, assuming a Lambertian emission profile (for the luminance measurements). Photovoltaic mode measurements were recorded under ∼100 mW/cm^2 solar light illumination simulated from a Xe lamp equipped with an AM 1.5G filter.

3. RESULTS AND DISCUSSION

3.1. PLEDs Performance. The PLEDs with structure glass/ITO/PEDOT:PSS (40 nm)/F8BT (90 nm)/triphenylsulfonium (TPS) salt/Al (150 nm) and the materials used are depicted in Figure 1. The J−V, luminance−voltage (L−V), and luminous efficiency−current density (L−J) characteristics of the PLEDs with two types of TPS-salts differing slightly in the anion size (i.e., triflate and nonaflate anions), which were deposited on top of the F8BT emitting layer, are shown in Figure 2. Both TPS-salts were spin-coated from their solution

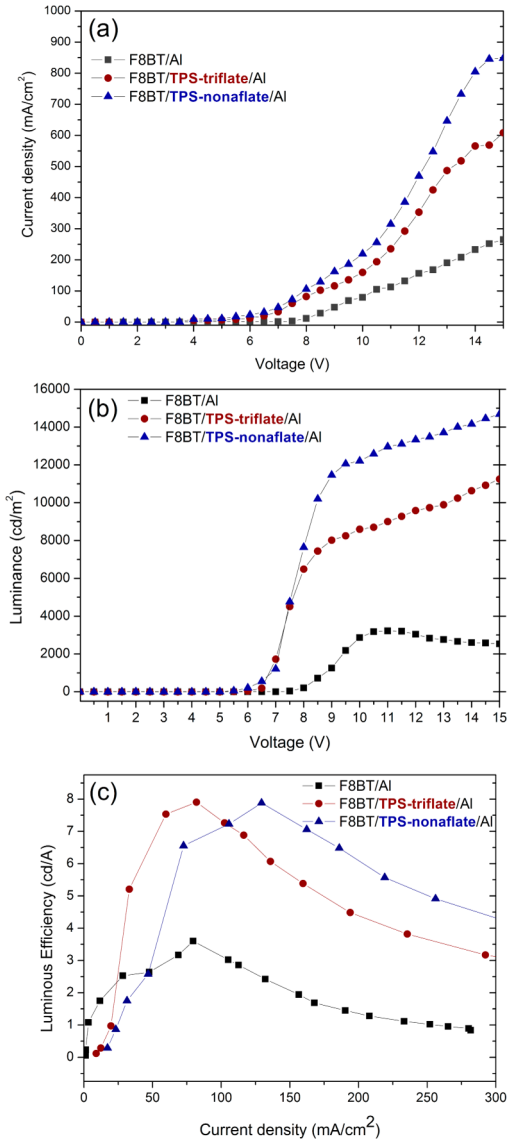

Figure 2. (a) Current density−voltage, (b) luminance−voltage, and (c) luminous efficiency−current density of PLEDs with structure glass/ITO/PEDOT:PSS (40 nm)/F8BT (90 nm)/triphenylsulfonium (TPS) salt/Al (150 nm) along with the reference device without the TPS-salt interlayer.

in methanol (an orthogonal solvent toward the underlying F8BT emitting layer), and the results presented in Figure 2 refer to optimized devices, obtained after fine-tuning of the processing conditions (solution concentration, spin-speed), as will be explained in detail in the morphology study (vide infra). The first striking observation is that the maximum luminance (Figure 2b) is almost quadrupled for the devices with the TPS-salts CILs (∼11 250 cd/m^2 for TPS-triflate and ∼14 682 cd/m^2 for TPS-nonaflate compared to ∼3221 cd/m^2 for the reference device without a CIL), while the current density (Figure 2a) shows an about 3-fold increase (from 265 mA/cm^2 for the reference device to 608 and 848 mA/cm^2 for the PLEDs with TPS-triflate and TPS-nonaflate, respectively; see also Table 1). Accordingly, Figure 2c shows that the luminous efficiencies of the PLEDs with the TPS-salt modified cathodes are both close

Table 1. Device Characteristics of PLEDs with the Structure ITO/PEDOT:PSS/F8BT/Cathode

cathode	V_{on} [V]	J_{max} [mA/cm^2]	L_{max} [cd/m^2]	luminous efficiency max [cd/A]	EQE$_{max}$ %	power efficiency max [lum/W]
Al	6.5	265	3221	2.4 (@ 10 V)	0.79	1.13 (@ 10 V)
TPS-triflate/Al	5.0	608	11 250	7.9 (@ 8 V)	2.60	3.15 (@ 7.5 V)
TPS-nonaflate/Al	5.0	848	14 682	7.8 (@ 8.5 V)	2.57	2.90 (@ 8.5 V)

to 7.85 cd/A (at 8 V), whereas the highest efficiency measured for the reference device was 2.4 cd/A (at 10 V). These values are comparable to those reported recently for all-organic thin F8BT-based PLEDs with zwitterionic conjugated polymers[53] or anionic CPEs[54] as EILs and very close to those obtained for 200 nm thick F8BT PLEDs with Ca/Al cathode.[55] Additionally, the turn-on voltage (defined here at $L \approx 10$ cd/m^2) is reduced from 6.5 V for the reference PLED to 5.0 V for PLEDs with the TPS-salts CILs, a result which is indicative of improved electron injection, since the anode side is similar in all devices. It is also noteworthy that the electroluminescence spectra are not affected by the insertion of these interfacial layers, all being identical to the typical F8BT emission spectrum (not shown). This means that no excited state bimolecular species is being formed at the polymer/TPS-salt interface as has been previously reported for the CN-PPP:TPS-salts blend.[50,51]

3.2. TPS-Salts Energy Level Determination and DFT Calculations. As a first step, in order to shed light to the functionality of these interlayers, the orbital energy levels of the TPS-salts should be discussed. These were estimated experimentally by applying a combination of spectroscopic and electrochemical techniques. More specifically, the ultraviolet photoelectron spectra (UPS) of the two TPS-salts with different anions (Figure 3a and b), which were spin-coated from a highly concentrated chloroform solution in order to form thick films on Al-coated Si substrates, reveal that the highest occupied molecular orbital (HOMO) energies of TPS-triflate and TPS-nonaflate lie at ca. 2.9 and 3.1 eV (±0.1 eV), respectively, relative to the Fermi level (see valence band edge in Figure 3b). In addition, the work function of each salt was estimated from the high binding energy (BE) cutoff region of these spectra (Figure 3a) to lay at about 4.8 and 4.5 eV, respectively. Thus, ionization potentials of about 7.7 eV for TPS-triflate and 7.6 eV (±0.1 eV) for TPS-nonaflate are calculated. By subtracting the 4.4 eV optical gap, as derived by the optical absorption spectra of the same films (Figure 3c), we calculate a LUMO level at about 3.3 and 3.2 eV (±0.1 eV), respectively. This is in fine accordance with cyclic voltammetry data of the TPS-salts solutions in acetonitrile (Figure 3d), depicting an irreversible reduction potential close to 1.6 V (vs SCE reference electrode)[56] for both TPS-triflate and TPS-nonaflate, which also translates to an experimental LUMO energy of about 3.2 eV. The electronic structure of the different TPS-salts is currently under investigation by DFT[57] and TD-DFT[58] calculations employing the M062X functional[59,60] and the 631-G11+(d,p) basis set with the aid of Gaussian 09.[61] The outcome of the theoretical study will be presented in detail elsewhere. Of particular relevance to the present work are the results of the above calculations on the neutral, that is, [TPS-X], versus the reduced form of the TPS-salts, that is, [TPS-X]$^-$. In particular, it was found that the total energy of the neutral ion-couple [TPS-X] is higher than that of its corresponding reduced form [TPS-X]$^-$, obtained when an electron is added to the TPS LUMO. More specifically, it was calculated that the reduced forms of TPS-triflate and TPS-nonaflate are more stable than the corresponding neutrals by 1.24 and 1.32 eV,

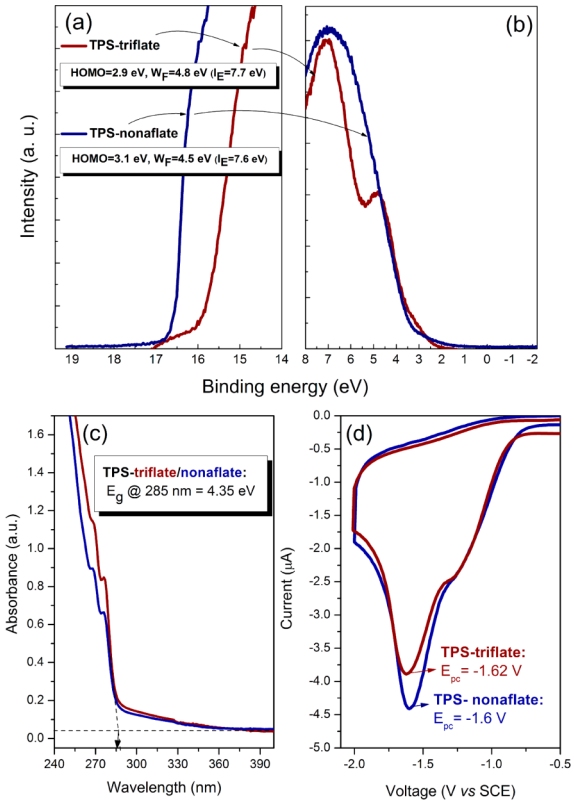

Figure 3. TPS-salts energy levels determination: ionization energies were determined by adding the work function estimated from the high binding energy cutoff region (a) and the HOMO from the low binding energy region, near the Fermi level (b), as both derived from the UPS spectra of TPS-salts thick films (top). LUMO energies were calculated either by subtracting the energy gap estimated from the UV−vis absorption spectra (small differences in absorbance are due to slightly different film thicknesses) (c) from the previously calculated ionization potentials or directly from the reduction potentials measured with cyclic voltammetry in acetonitrile solution (d).

respectively. Note that these calculations were carried out on isolated systems of the TPS-salts, namely, without taking into account any solvent interactions. The theoretical investigation of the reduction of TPS cation (TPS$^+$) alone, always results in its decomposition, in agreement with the well-established experimental data on TPS electrochemical reduction.[62] However, the neutral ion couple [TPS-X], which actually resembles the salt in the solid state, is found to be stable toward reduction. Similar results confirming the stability of TPS-salts upon reduction have been recently reported also by another theoretical research group.[63] In Figure 4, electron density plots show that the LUMO of [TPS-X] and the HOMO of [TPS-X]$^-$ are very similar. This is important information, meaning that the reduced form is further stabilizing the TPS-salt molecule rather than leading to its dissociation, highlighting the suitability of these compounds to be incorporated as electron injecting layers in organic electronic devices. This finding is also supportive to our previously expressed claim against TPS-salt

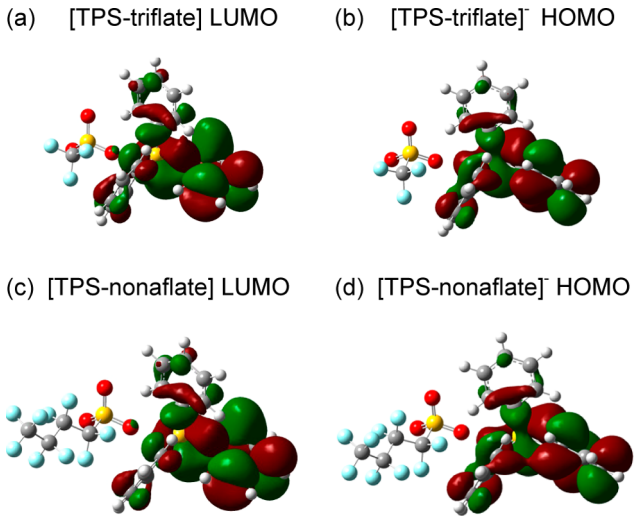

Figure 4. Electron density plots of the LUMO of the neutral TPS-salts (a,c) and the HOMO of their corresponding reduced forms (b,d), showing that the latter are being formed by the addition of an electron into the LUMO of the neutrals.

decomposition upon electron transfer from the polymer or the electrode, when the salt was inserted in the blue-emitting polymer CN-PPP.[50,51] The experimental evidence to that was given by the emergence of an emission peak attributed to a bimolecular species, that is, an electroplex, the formation of which required an electron to be placed at the TPS LUMO and a hole at the polymer HOMO. In addition to that, in the present work, we noticed that the TPS-salt modified PLED devices exhibited a similar temporal stability upon sequential scans to the reference device without the cathode interfacial layer.

By taking into consideration the orbital energies of each material and the work function of the electrodes that are being shown in the band diagram sketched in Figure 5a, one would expect a slightly increased barrier for electron injection and accordingly, a deteriorated device performance may be anticipated when the sulfonium salt layer is inserted. More specifically, the electron injection barrier between Al cathode and TPS molecules is ca. 1.1 eV, a high value for efficient electron injection and indeed higher than that of the unmodified F8BT/Al interface (0.8 eV). On the other hand, the theoretical calculations showed that the insertion of an electron to the TPS-salt LUMO stabilizes their orbitals by about 1.3 eV (vide supra). This would literally mean that the lowering of the LUMO energy upon electron injection would ideally result in a perfect alignment of the TPS-salt LUMO with the Al Fermi level and the formation of an ohmic contact with the electrode, thus justifying the experimental findings presented in Figure 2. In order to clarify further the injection mechanism, we performed photovoltaic measurements on the same devices as in Figure 2 with the aim to determine the built-in potential across the diode. Figure 5b shows the open circuit voltage (V_{oc}) for the devices without (reference) and with the TPS-salts modified Al cathode. The value obtained for the reference device ($V_{oc} \approx 1.0$ V) represents the energy difference between the two electrodes (ITO/PEDOT:PSS anode and Al cathode) and is in good agreement with previous results with these materials.[6,21] Upon incorporating TPS-triflate or TPS-nonaflate at the F8BT/Al interface, the V_{oc} is shifted to higher voltage (V_{oc} = 1.4−1.5 V). This indicates an increase of the internal built-in potential upon modifying the Al/F8BT interface with the TPS salt and, thus, a lowering of the effective

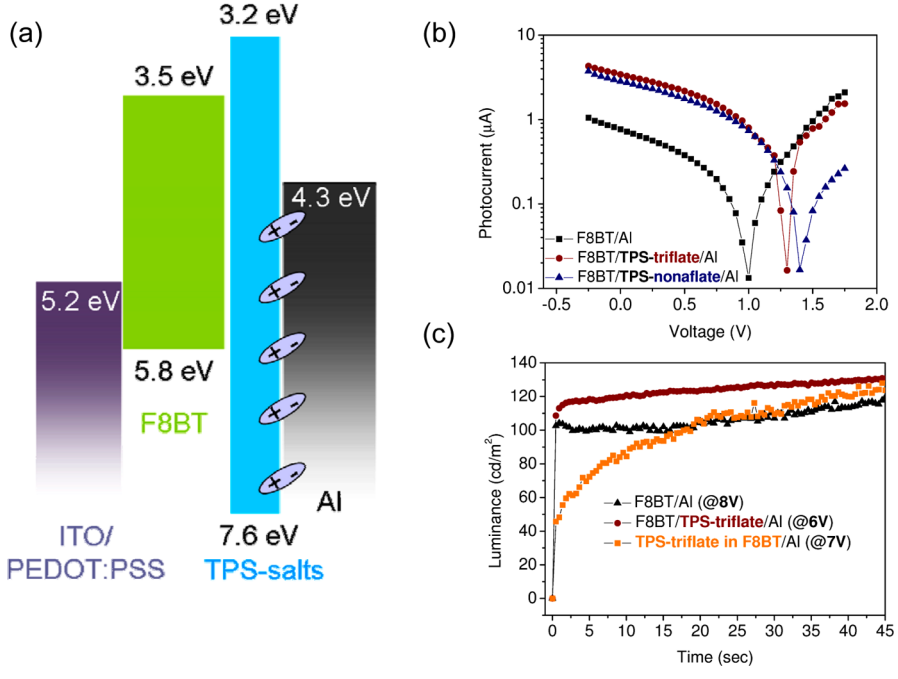

Figure 5. (a) Energy level diagram showing also the orientation of the dipole formed upon electron injection to the TPS-salt/Al interface. The orbital energies of F8BT and the work function of the electrodes are based on literature values, whereas the HOMO−LUMO energies of the TPS-salts are calculated in this work (see Figure 3 above). (b) Photovoltaic measurements of the TPS-salts modified PLEDs. (c) Time response of luminance for the devices with an Al and TPS-triflate/Al cathode. The EL time response of a PLED with TPS-triflate doped F8BT as the active layer is also shown for comparison.

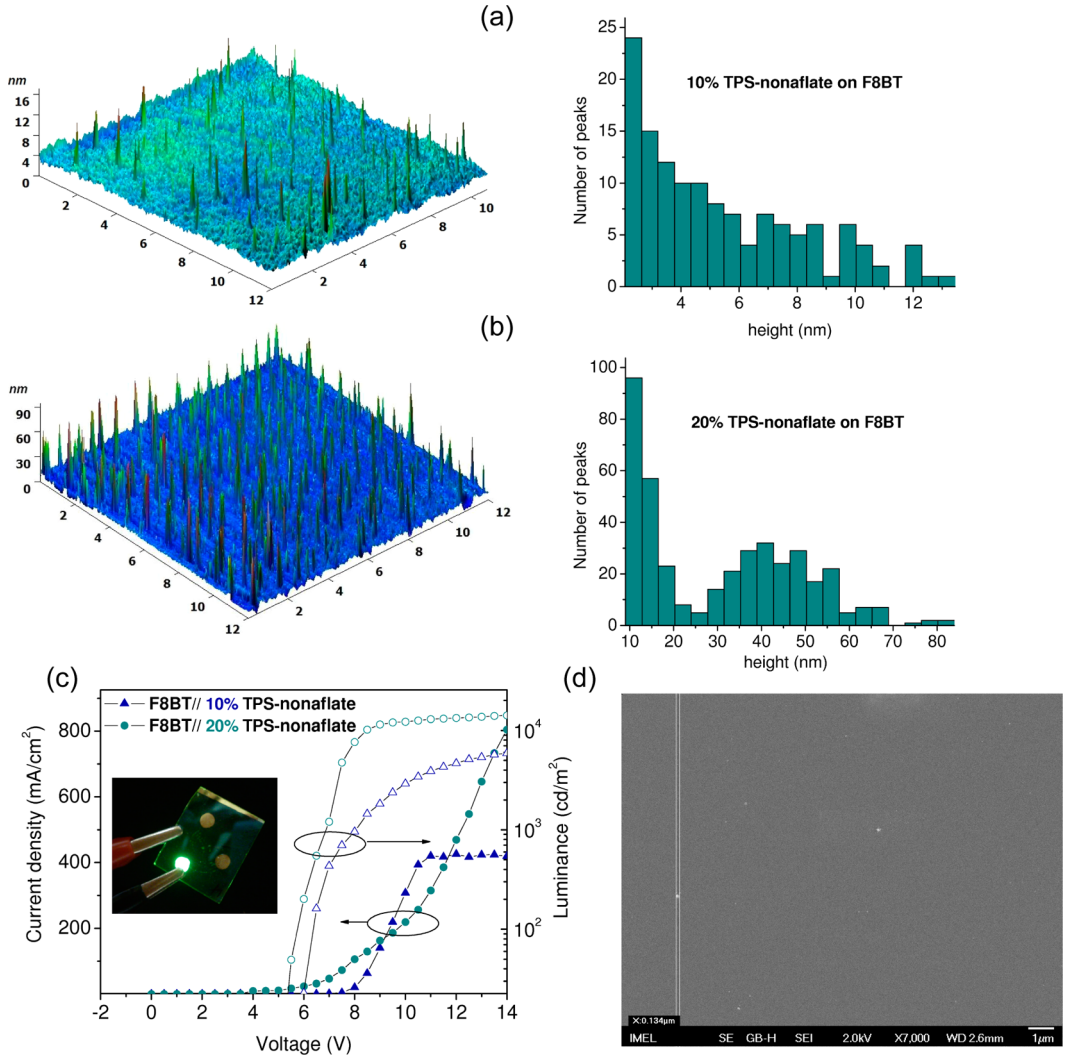

Figure 6. AFM images (12 × 12 μm^2) depicting the 3D topography of two F8BT/TPS-nonaflate films, where the TPS-salt was deposited on F8BT polymer substrate from (a) 10% w/v and (b) 20% w/v concentration solutions in MeOH (left), and the respective statistical analysis of their height distributions (right). (c) Current density–voltage (closed symbols) and luminance–voltage (open symbols) characteristics of the PLEDs incorporating the above shown TPS-nonaflate interlayers. Inset: Photograph of the respective operating device. (d) SEM image of an F8BT film with TPS-nonaflate (10% w/v) deposited on top.

injection barrier height for this device architecture. The latter is in accordance with the preceding argumentation, leading obviously to a more balanced charge injection, ultimately resulting in enhanced luminance and quantum efficiency. Note that similar results have been obtained with conjugated polyelectrolytes (CPEs) acting as electron injecting layers.[6,64] Here also, in accordance with the pioneering work by Wu et al.,[64] the V_{oc} shift is attributed to the formation (due to the polarity induced by triphenylsulfonium cation and the counterions) of a negative interfacial dipole with the positive pole directed toward the organic and the negative pole toward the metal, forming thus a negative potential for electron injection.[65] Therefore, this mechanism could be rationalized as interfacial dipole assisted electron injection at the Al/TPS interface. The above-described dipole is also sketched in Figure 5a. Note that the deep lying HOMO level of the TPS-salts could also contribute to the enhancement of the PLED performance due to a potential hole blocking effect, given that the energetic barrier of hole transfer from the F8BT HOMO to that of the TPS-salt is about 1.8 eV.

At this point, we would like to notice that, since TPS-salts actually constitute ionic compounds, ion motion into the conjugated polymer resulting in an electrochemical doping process should be also considered as a possible operational mechanism.[28] For this reason, we performed transient measurements in the PLED devices to get information about the device response time.[66] The electroluminescence transients of the respective PLEDs were recorded at a voltage slightly higher than the turn-on voltage of each device (specifically at a luminance value ≈ 120 cd/m^2) and are presented in Figure 5c. They reveal that the response time of the TPS-salt modified devices is very similar to that of the reference device with an F8BT/Al cathode; namely, they both lay in the subsecond time scale. Furthermore, to exclude the possibility of electrochemical doping taking place at the interface, we present in the same graph the transient EL data of a PLED with the TPS-triflate salt blended with F8BT copolymer inside the active layer, which should be characteristic of a doping mechanism. Although, also in this device, the response time is still very short, as argued in our previous work,[49] the difference between the two types of devices is obvious. Therefore, from the above, it becomes clear

that the electrochemical doping during operation should be ruled out upon deposition of TPS-salts on top of F8BT emitting layer.

3.3. Investigation of the TPS-Salts Film Morphology. The film morphology is a crucial parameter that has to be accounted for when introducing interfacial layers in optoelectronic devices. On the other hand, triphenylsulfonium salts have been so far used as additives blended inside a polymer matrix and their film forming properties have not been explored in detail yet. For this reason, we studied extensively with atomic force microscopy (AFM) and scanning electron microscopy (SEM) the surface topography of both TPS-salts deposited on F8BT underlayer from their methanolic solutions at various concentrations (the spin speed was kept constant at 2000 rpm). A representative example of this study is presented in Figure 6, which depicts the 3D topography of TPS-nonaflate interlayers spin-coated from their 10% (Figure 6a) and 20% w/v (Figure 6b) solutions in MeOH on the F8BT polymer. It can be seen that the F8BT surface is not fully covered with the TPS-salt, even when it is spin-coated from relatively dense solutions (20% w/v corresponds to 200 mg/mL); instead the TPS-salt forms agglomerates with a moundlike geometry that tend to grow higher and bigger as the solution concentration increases. By analyzing further these AFM images, it can be derived that, upon doubling the solution concentration from 10% to 20% w/v, there is a 5-fold increase in the polymer surface coverage (from 0.4% to 2.1%). This increase seems to be attributed more to the larger density of the TPS-salt agglomerates at high concentrations (2.8 vs 1.1 μm^{-2} at 10% w/v) and less to the growth of their lateral size, which goes from ~70 to ~95 nm (mean width values at 10% and 20% w/v, respectively). Quite interestingly, a significant change in the height of the TPS-nonaflate agglomerates is observed from the analysis of the AFM images. More specifically, from the height distribution plots, shown also in Figure 6a and b, it can be seen that most of the features detected with AFM in the case of the 10% w/v TPS-nonaflate are between 1 and 10 nm in height, whereas a bimodal distribution occurs for deposition from the higher concentration solution, corresponding to agglomerates ranging from 10 to 20 nm and 30 to 60 nm in height.

The above are correlated with the respective devices performance, which is shown in Figure 6c. It can be deduced that both current density and luminance are higher when the TPS-nonaflate interlayer is deposited from the denser solution. Note that, by further increasing the concentration of the solution (>20% w/v), the current density remains high but the luminance drops gradually (not shown here), indicating a disruption in the charge balance of the device. A photograph of the operating device (inset) which reveals a homogeneous emission of the PLED is also shown. Finally, Figure 6d depicts the top view of the surface of TPS-nonaflate on F8BT polymer as recorded with SEM, which is though less informative than the respective AFM images (the nanometer-sized clusters could not be easily detected due to charging effects).

In contrast to the above SEM image, the situation was totally different when TPS-triflate was deposited on top of F8BT, as revealed by the representative SEM images of TPS-triflate deposited from three different concentration solutions on F8BT films, which are presented in Figure 7. Here also, there is a tendency of the TPS-salt agglomerates to increase in size and number with solution concentration. From the analysis of these images, a bimodal distribution of the agglomerates width is calculated for all concentrations, with most of them ranging

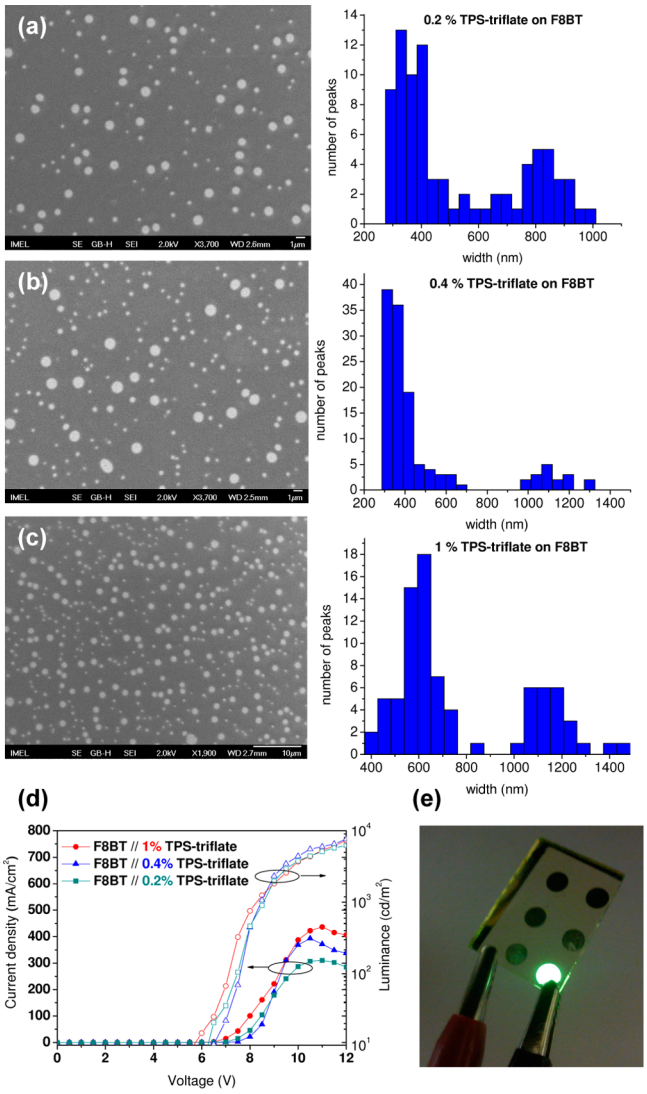

Figure 7. SEM images of TPS-triflate on F8BT spin-coated from their (a) 0.2%, (b) 0.4%, and (c) 1% w/v solutions in MeOH and the width distribution of the agglomerates, all calculated from a 23 × 23 μm^2 area of the above images (notice the smaller magnification of image (c)). (d) Current density–voltage (closed symbols) and luminance–voltage (open symbols) characteristics of F8BT-based PLEDs with the above shown TPS-triflate interlayers. (e) Photograph of the operating PLED device incorporating a TPS-triflate cathode modifier.

around 400–600 nm and a smaller number being over 1 μm. Note that in the case of TPS-triflate, the SEM images provide a better overview of the surface topography than the ones measured with AFM (not shown), since the large height differences result in uncontrolled AFM tip oscillations and therefore images with inaccurate information. From the analysis of the SEM images, we found that the coverage of F8BT with TPS-triflate aggregates increases from 4.1% to 5.9% and further to 8.2% as the concentration of the initial solution increases from 0.2% (Figure 7a) to 0.4% (Figure 7b) and finally to 1% w/v (Figure 7c), respectively. The *J*–*V*–*L* characteristics of the respective PLED devices are presented in Figure 7d. In this concentration range, the device performance is only marginally affected by the TPS-triflate solution concentration. However, a somewhat better performance for the device comprising the TPS-triflate interlayer deposited from the 1% w/v solution can be discerned. Again, by further increasing the concentration

(above 1% w/v), the overall performance starts to deteriorate. Here it should be also noted that, since the size of the TPS-triflate agglomerates is close to the wavelength of the light emitted by F8BT polymer, optical effects may also contribute to the observed luminance. Nonetheless, the macroscopically perceived emission of the PLED is totally homogeneous as revealed in the photograph shown in Figure 7e.

A pronounced difference between the TPS-triflate and TPS-nonaflate layers when deposited on F8BT substrate is the substantially different solution concentrations that lead to relatively high surface coverage and optimum device performance for each salt. In particular, while we observe that the relatively dense (15−20% w/v) TPS-nonaflate solutions are the ones showing the best performance, in the case of TPS-triflate interlayers, the optimum solutions are below 1% w/v. This is directly related to the affinity of each TPS-salt toward the F8BT polymer substrate. It can be concluded that the nature of the anion influences its ability to wet the polymeric substrate. In particular, the higher the degree of fluorination of the anion (nonaflate vs triflate), the better the wettability of the hydrophobic F8BT, as surface energies are matched more evenly. Indeed, the contact angles of droplets cast from 100 mg/mL TPS-nonaflate and 60 mg/mL TPS-triflate solutions in methanol on an F8BT film are measured to be 15° and 23°, respectively, whereas pure methanol drop-cast on F8BT had a contact angle of 42°. This explains why TPS-triflate tends to form large size agglomerates and, eventually, dewets from the substrate as the concentration increases, whereas the TPS-nonaflate is homogeneously distributed on F8BT underlayer at very high concentration solutions, while it hardly covers the surface when spin-coated from very dilute solutions. All the above highlight the importance of finding the optimum processing conditions for each material that is being used as interfacial layer, especially when it is deposited from solution (in the case of vacuum evaporated materials, the most critical parameter that should be finely tuned is typically the film thickness).

From the above study, we conclude that complete coverage of the emitting layer is not always a prerequisite for optimal performance, a conclusion that has been implied also by other groups.[67,68] In fact, we showed that a morphology characterized by a large number of relatively small size TPS-salt agglomerates, evenly distributed on the F8BT layer, is desirable for highly efficient PLEDs.

4. CONCLUSIONS

We have demonstrated for the first time the use of triphenylsulfonium salts as cathode interfacial layers in F8BT-based PLEDs with an Al cathode. The inclusion of TPS-triflate or TPS-nonaflate between the emissive layer and the electrode resulted in brighter devices, substantial improvement in the luminance efficiencies, and lower turn-on and operating voltage. This was primarily attributed to a reduction in the barrier posed for electron injection as well as to the efficient charge transport through the TPS sites. DFT calculations showed that electron transfer to the TPS-salt molecules is stabilizing instead of dissociating the neutral compound. Additionally, open circuit voltage measurements and studies about the electroluminescence response time of the PLEDs gave an insight to the possible mechanism of operation, which may be explained by considering a modification of the cathode effective work function due to dipole formation at the metal/organic interface rather than ion motion and electrochemical doping at the interface. The net effect is a shift in the vacuum level and concomitant improvement of electron injection. Furthermore, a key processing parameter was proven to be the obtained film morphology, since the formation of homogeneously dispersed agglomerates with a moundlike geometry is beneficial for electron injection and transport to the emitting layer. The presented results successfully introduce TPS-salts as solution-processable cathode interfacial layers and pave the way for the alternative utilization of this wide class of materials in other than patterning applications in optoelectronic devices.

AUTHOR INFORMATION

Corresponding Authors

*E-mail: dgeorg@imel.demokritos.gr (D.G.G.).
*E-mail: argitis@imel.demokritos.gr (P.A.).

Notes

The authors declare no competing financial interest.

ACKNOWLEDGMENTS

This research was financed by the European Commission by FP7-REGPOT-2009-245940, Project MiNaSys-CoE, Micro and Nano Systems - Center of Excellence. D.G.G. is grateful to C. Skoulikidou for recording the SEM images and A. Soultati for her help with the contact angle measurements.

REFERENCES

(1) Zheng, H.; Zheng, Y.; Liu, N.; Ai, N.; Wang, Q.; Wu, S.; Zhou, J.; Hu, D.; Yu, S.; Han, S.; Xu, W.; Luo, C.; Meng, Y.; Jiang, Z.; Chen, Y.; Li, D.; Huang, F.; Wang, J.; Peng, J.; Cao, Y. *Nat. Commun.* **2013**, *4*, 1971.
(2) Stossel, M.; Staudigel, J.; Steuber, F.; Simmerer, J.; Wittmann, G.; Kanitz, A.; Klausmann, H.; Rogler, W.; Roth, W.; Schumann, J.; Winnacker, A. *Phys. Chem. Chem. Phys.* **1999**, *1*, 1791−1793.
(3) Hung, L. S.; Tang, C. W.; Mason, M. G. *Appl. Phys. Lett.* **1997**, *70*, 152−154.
(4) Brown, T. M.; Friend, R. H.; Millard, I. S.; Lacey, D. J.; Burroughes, J. H.; Cacialli, F. *Appl. Phys. Lett.* **2001**, *79*, 174−176.
(5) Cho, K.; Cho, S. W.; Jeon, P. E.; Lee, H.; Whang, C. N.; Jeong, K.; Kang, S. J.; Yi, Y. *Appl. Phys. Lett.* **2008**, *92*, 93304.
(6) Xie, K.; Qiao, J.; Duan, L.; Li, Y.; Zhang, D.; Dong, G.; Wang, L.; Qiu, Y. *Appl. Phys. Lett.* **2008**, *93*, 183302.
(7) Ma, L.; Xie, Z. Y.; Liu, J.; Yang, J. W.; Cheng, Y. X.; Wang, L. X.; Wang, F. S. *Appl. Phys. Lett.* **2005**, *87*, 163502.
(8) Yi, Y. J.; Kang, S. J.; Cho, K.; Koo, J. M.; Han, K.; Park, K.; Noh, M.; Whang, C. N.; Jeong, K. *Appl. Phys. Lett.* **2005**, *86*, 213502.
(9) Li, Y.; Zhang, D. Q.; Duan, L.; Zhang, R.; Wang, L. D.; Qiu, Y. *Appl. Phys. Lett.* **2007**, *90*, 12119.
(10) Tokmoldin, N.; Griffiths, N.; Bradley, D. D. C.; Haque, S. A. *Adv. Mater.* **2009**, *21*, 3475−3478.
(11) Vasilopoulou, M.; Kennou, S.; Ladas, S.; Georga, S. N.; Botzakaki, M.; Skarlatos, D.; Krontiras, C. A.; Stathopoulos, N. A.; Argitis, P.; Palilis, L. C. *Org. Electron.* **2013**, *14*, 312−319.
(12) Bolink, H. J.; Coronado, E.; Repetto, D.; Sessolo, M. *Appl. Phys. Lett.* **2007**, *91*, 223501.
(13) Vasilopoulou, M.; Palilis, L. C.; Georgiadou, D. G.; Douvas, A. M.; Argitis, P.; Kennou, S.; Sygellou, L.; Papadimitropoulos, G.; Kostis, I.; Stathopoulos, N. A.; Davazoglou, D. *Adv. Funct. Mater.* **2011**, *21*, 1489−1497.
(14) Vasilopoulou, M.; Palilis, L. C.; Georgiadou, D. G.; Argitis, P.; Kennou, S.; Sygellou, L.; Kostis, I.; Papadimitropoulos, G.; Konofaos, N.; Iliadis, A. A.; Davazoglou, D. *Appl. Phys. Lett.* **2011**, *98*, 123301.
(15) Palilis, L. C.; Uchida, M.; Kafafi, Z. H. *IEEE J. Sel. Top. Quantum Electron.* **2004**, *10*, 79−88.
(16) Li, N.; Wang, P. F.; Lai, S. L.; Liu, W. M.; Lee, C. S.; Lee, S. T.; Liu, Z. T. *Adv. Mater.* **2010**, *22*, 527−530.

(17) Sasabe, H.; Tanaka, D.; Yokoyama, D.; Chiba, T.; Pu, Y. J.; Nakayama, K.; Yokoyama, M.; Kido, J. *Adv. Funct. Mater.* **2011**, *21*, 336−342.
(18) Lee, H.; Cho, G.; Woo, S.; Nam, S.; Jeong, J.; Kim, H.; Kim, Y. *RSC Adv.* **2012**, *2*, 8762−8767.
(19) Huang, J. S.; Li, G.; Wu, E.; Xu, Q. F.; Yang, Y. *Adv. Mater.* **2006**, *18*, 114−117.
(20) Lu, L. P.; Kabra, D.; Friend, R. H. *Adv. Funct. Mater.* **2012**, *22*, 4165−4171.
(21) Palilis, L. C.; Vasilopoulou, M.; Georgiadou, D. G.; Argitis, P. *Org. Electron.* **2010**, *11*, 887−894.
(22) Palilis, L. C.; Vasilopoulou, M.; Douvas, A. M.; Georgiadou, D. G.; Kennou, S.; Stathopoulos, N. A.; Constantoudis, V.; Argitis, P. *Sol. Energy Mater. Sol. Cells* **2013**, *114*, 205−213.
(23) Vasilopoulou, M.; Georgiadou, D. G.; Douvas, A. M.; Soultati, A.; Constantoudis, V.; Davazoglou, D.; Gardelis, S.; Palilis, L. C.; Fakis, M.; Kennou, S.; Lazarides, T.; Coutsolelos, A. G.; Argitis, P. *J. Mater. Chem. A* **2013**, DOI:10.1039/c3ta13107f (assess date: 18th October 2013).
(24) Guo, T. F.; Yang, F. S.; Tsai, Z. J.; Wen, T. C.; Hsieh, S. N.; Fu, Y. S. *Appl. Phys. Lett.* **2005**, *87*, 13504.
(25) Guo, T. F.; Yang, F. S.; Tsai, Z. J.; Wen, T. C.; Hsieh, S. N.; Fu, Y. S.; Chung, C. T. *Appl. Phys. Lett.* **2006**, *88*, 113501.
(26) Cho, K.; Cho, S. W.; Whang, C. N.; Jeong, K.; Kang, S. J.; Yi, Y. *Appl. Phys. Lett.* **2007**, *91*, 152107.
(27) Hsiao, C. C.; Hsiao, A. E.; Chen, S. A. *Adv. Mater.* **2008**, *20*, 1982−1988.
(28) Sandström, A.; Matyba, P.; Inganäs, O.; Edman, L. *J. Am. Chem. Soc.* **2010**, *132*, 6646−6647.
(29) Wu, J. S.; Lu, H. H.; Hung, W. C.; Lin, G. H.; Chen, S. A. *Appl. Phys. Lett.* **2010**, *97*, 23304.
(30) Chen, Z.; Niu, Q. L.; Zhang, Y.; Ying, L.; Peng, J. B.; Cao, Y. *ACS Appl. Mater. Interfaces* **2009**, *1*, 2785−2788.
(31) Guan, X.; Zhang, K.; Huang, F.; Bazan, G. C.; Cao, Y. *Adv. Funct. Mater.* **2012**, *22*, 2846−2854.
(32) Zhou, Y. H.; Fuentes-Hernandez, C.; Shim, J.; Meyer, J.; Giordano, A. J.; Li, H.; Winget, P.; Papadopoulos, T.; Cheun, H.; Kim, J.; Fenoll, M.; Dindar, A.; Haske, W.; Najafabadi, E.; Khan, T. M.; Sojoudi, H.; Barlow, S.; Graham, S.; Bredas, J. L.; Marder, S. R.; Kahn, A.; Kippelen, B. *Science* **2012**, *336*, 327−332.
(33) Duarte, A.; Pu, K. Y.; Liu, B.; Bazan, G. C. *Chem. Mater.* **2011**, *23*, 501−515.
(34) Hu, S.; Zhong, C.; Wu, H.; Cao, Y. *Conjugated Polyelectrolytes: Fundamentals and Applications*, First ed.; Liu, B., Bazan, G. C., Eds.; Wiley-VCH Verlag GmbH & Co. KGaA: Weinheim, 2013; pp 345−388.
(35) Duan, C. H.; Zhang, K.; Guan, X.; Zhong, C. M.; Xie, H. M.; Huang, F.; Chen, J. W.; Peng, J. B.; Cao, Y. *Chem. Sci.* **2013**, *4*, 1298−1307.
(36) Gutacker, A.; Adamczyk, S.; Helfer, A.; Garner, L. E.; Evans, R. C.; Fonseca, S. M.; Knaapila, M.; Bazan, G. C.; Burrows, H. D.; Scherf, U. *J. Mater. Chem.* **2010**, *20*, 1423−1430.
(37) Ying, L.; Zalar, P.; Collins, S. D.; Chen, Z.; Mikhailovsky, A. A.; Nguyen, T. Q.; Bazan, G. C. *Adv. Mater.* **2012**, *24*, 6496−6501.
(38) Lim, G. E.; Ha, Y. E.; Jo, M. Y.; Park, J.; Kang, Y. C.; Kim, J. H. *ACS Appl. Mater. Interfaces* **2013**, *5*, 6508−6513.
(39) Min, C.; Shi, C. S.; Zhang, W. J.; Jiu, T. G.; Chen, J. S.; Ma, D. G.; Fang, J. F. *Angew. Chem., Int. Ed.* **2013**, *52*, 3417−3420.
(40) Hsieh, S. N.; Hsiao, S. W.; Chen, T. Y.; Li, C. Y.; Lee, C. H.; Guo, T. F.; Hsu, Y. J.; Lin, T. L.; Wei, Y.; Wen, T. C. *J. Mater. Chem.* **2011**, *21*, 8715−8720.
(41) Liu, G.; Li, Y. H.; Tan, W. Y.; He, Z. C.; Wang, X. T.; Zhang, C.; Mo, Y. Q.; Zhu, X. H.; Peng, J. B.; Cao, Y. *Chem.—Asian J.* **2012**, *7*, 2126−2132.
(42) Stewart, J. S.; Lippert, T.; Nagel, M.; Nuesch, F.; Wokaun, A. *Appl. Phys. Lett.* **2012**, *100*, 203303.
(43) Shaw-Stewart, J. R. H.; Mattle, T.; Lippert, T. K.; Nagel, M.; Nuesch, F. A.; Wokaun, A. *J. Appl. Phys.* **2013**, *113*, 43104.
(44) Crivello, J. V.; Lam, J. H. W. *J. Polym. Sci, Part A: Polym. Chem.* **1979**, *17*, 1047−1057.
(45) MacDonald, S. A.; Willson, C. G.; Frechet, J. M. J. *Acc. Chem. Res.* **1994**, *27*, 151−158.
(46) Reichmanis, E.; Houlihan, F. M.; Nalamasu, O.; Neenan, T. X. *Chem. Mater.* **1991**, *3*, 394−407.
(47) Vasilopoulou, M.; Georgiadou, D.; Pistolis, G.; Argitis, P. *Adv. Funct. Mater.* **2007**, *17*, 3477−3485.
(48) Georgiadou, D. G.; Vasilopoulou, M.; Pistolis, G.; Palilis, L.; Dimotikali, D.; Argitis, P. *Phys. Status Solidi A* **2008**, *205*, 2526−2531.
(49) Georgiadou, D. G.; Palilis, L. C.; Vasilopoulou, M.; Pistolis, G.; Dimotikali, D.; Argitis, P. *J. Mater. Chem.* **2011**, *21*, 9296−9301.
(50) Georgiadou, D. G.; Palilis, L. C.; Vasilopoulou, M.; Pistolis, G.; Dimotikali, D.; Argitis, P. *RSC Adv.* **2012**, *2*, 11786−11792.
(51) Georgiadou, D. G.; Palilis, L. C.; Vasilopoulou, M.; Pistolis, G.; Dimotikali, D.; Argitis, P. *Synth. Met.* **2013**, *181*, 37−44.
(52) Loutfy, R. O.; Still, I. W. J.; Thompson, M.; Leong, T. S. *Can. J. Chem.* **1979**, *57*, 638−644.
(53) Fang, J. F.; Wallikewitz, B. H.; Gao, F.; Tu, G. L.; Muller, C.; Pace, G.; Friend, R. H.; Huck, W. T. S. *J. Am. Chem. Soc.* **2011**, *133*, 683−685.
(54) Zhu, X. G.; Xie, Y. H.; Li, X.; Qiao, X. F.; Wang, L.; Tu, G. L. *J. Mater. Chem.* **2012**, *22*, 15490−15494.
(55) Kabra, D.; Lu, L. P.; Song, M. H.; Snaith, H. J.; Friend, R. H. *Adv. Mater.* **2010**, *22*, 3194−3198.
(56) Vase, K. H.; Holm, A. H.; Norrman, K.; Pedersen, S. U.; Daasbjerg, K. *Langmuir* **2008**, *24*, 182−188.
(57) Parr, R. G.; Yang, W. T. *Annu. Rev. Phys. Chem.* **1995**, *46*, 701−728.
(58) Marques, M. A. L.; Gross, E. K. U. *Annu. Rev. Phys. Chem.* **2004**, *55*, 427−455.
(59) Zhao, Y.; Truhlar, D. G. *Acc. Chem. Res.* **2008**, *41*, 157−167.
(60) Zhao, Y.; Truhlar, D. G. *Theor. Chem. Acc.* **2008**, *120*, 215−241.
(61) Frisch, M. J.; Trucks, G. W.; Schlegel, H. B.; Scuseria, G. E.; Robb, M. A.; Cheeseman, J. R.; Scalmani, G.; Barone, V.; Mennucci, B.; Petersson, G. A.; Nakatsuji, H.; Caricato, M.; Li, X.; Hratchian, H. P.; Izmaylov, A. F.; Bloino, J.; Zheng, G.; Sonnenberg, J. L.; Hada, M.; Ehara, M.; Toyota, K.; Fukuda, R.; Hasegawa, J.; Ishida, M.; Nakajima, T.; Honda, Y.; Kitao, O.; Nakai, H.; Vreven, T.; Montgomery, J. A.; Peralta, J. E.; Ogliaro, F.; Bearpark, M.; Heyd, J. J.; Brothers, E.; Kudin, K. N.; Staroverov, V. N.; Kobayashi, R.; Normand, J.; Raghavachari, K.; Rendell, A.; Burant, J. C.; Iyengar, S. S.; Tomasi, J.; Cossi, M.; Rega, N.; Millam, J. M.; Klene, M.; Knox, J. E.; Cross, J. B.; Bakken, V.; Adamo, C.; Jaramillo, J.; Gomperts, R.; Stratmann, R. E.; Yazyev, O.; Austin, A. J.; Cammi, R.; Pomelli, C.; Ochterski, J. W.; Martin, R. L.; Morokuma, K.; Zakrzewski, V. G.; Voth, G. A.; Salvador, P.; Dannenberg, J. J.; Dapprich, S.; Daniels, A. D.; Farkas, Ö.; Foresman, J. B.; Ortiz, J. V.; Cioslowski, J.; Fox, D. J. *Gaussian 09*, Revision A.1; Gaussian, Inc.: Wallingford, CT, 2009.
(62) McKinney, P. S.; Rosenthal, S. *J. Electroanal. Chem. Interfacial Electrochem.* **1968**, *16*, 261−270.
(63) Endo, M.; Tagawa, S. *J. Photopolym. Sci. Technol.* **2011**, *24*, 205−210.
(64) Wu, H. B.; Huang, F.; Mo, Y. Q.; Yang, W.; Wang, D. L.; Peng, J. B.; Cao, Y. *Adv. Mater.* **2004**, *16*, 1826−1830.
(65) Lee, W.; Seo, J. H.; Woo, H. Y. *Polymer* **2013**, *54*, 5104−5121.
(66) Hoven, C.; Yang, R.; Garcia, A.; Heeger, A. J.; Nguyen, T. Q.; Bazan, G. C. *J. Am. Chem. Soc.* **2007**, *129*, 10976−10977.
(67) Yang, R. Q.; Xu, Y. H.; Dang, X. D.; Nguyen, T. Q.; Cao, Y.; Bazan, G. C. *J. Am. Chem. Soc.* **2008**, *130*, 3282−3283.
(68) Garcia, A.; Bakus, R. C.; Zalar, P.; Hoven, C. V.; Brzezinski, J. Z.; Nguyen, T. Q. *J. Am. Chem. Soc.* **2011**, *133*, 2492−2498.